ELSEVIER

Journal of Non-Crystalline Solids 287 (2001) 145–161

JOURNAL OF NON-CRYSTALLINE SOLIDS

www.elsevier.com/locate/jnoncrysol

Section 3. Stability and crystallization

# Nanocrystallization of metallic glasses

Tadeusz Kulik *

*Faculty of Materials Science and Engineering, Warsaw University of Technology, Wołoska 141, 02-507 Warsaw, Poland*

**Abstract**

The paper summarizes briefly the current status of research in the field of nanocrystallization of metallic glasses especially highlighting the influence of glass composition and conditions of devitrification process on size, morphology and composition of crystallization products. Conventional crystallization creates a nanocrystalline structure only in glasses with particular compositions. Any metallic glass, decomposing in a primary crystallization process, can be converted into partially nanocrystalline material using non-conventional methods of heat treatment, e.g. high-temperature or low-temperature nanocrystallization. Temperature of devitrification process influences sizes and compositions of crystallization products for any volume fraction of crystalline phase. The change of crystallites sizes can change their morphologies. The change of a crystallite composition usually affects the lattice parameter but also can result in a change of crystallographic structure of the same phase or in formation of another phase. Composition of primary crystallites is dependent on temperature as well as on time of devitrification process. The lower the annealing temperature and the shorter the annealing time (smaller crystallites) the more the crystallites composition differs from the equilibrium state. 

*PACS:* 81.05.Kf; 81.07.Bc; 81.40.Ef; 64.70.Kb

## 1. Introduction

Polycrystalline solids with grain size less than 100 nm are called nanocrystalline materials and can be produced using various methods and different starting phase: vapour (inert gas condensation, sputtering, plasma processing, vapour deposition), liquid (electrodeposition, rapid solidification) or solid (mechanical alloying, severe plastic deformation, spark erosion) [1–3]. Most of the methods offer two possibilities for creation of nanocrystalline structure: directly in one process or indirectly through an amorphous precursor. Nanocrystallization of metallic glasses is an example of the second procedure. In this case, nanocrystalline material is produced in two steps: (1) formation of amorphous state by quenching of liquid alloy, and (2) partial or complete crystallization of the amorphous alloy by annealing. Three important groups of nanocrystalline materials produced from metallic glasses can be distinguished: constructional Al-based alloys [4–11], magnetically soft [12–17] and magnetically hard [18–25] Fe-based alloys. Examples of the alloys compositions and main aspects of their structure are presented in Table 1. There are two basic parameters characterizing structure of these materials: crystallite diameter, $D$, and volume fraction, $V_{cr}$, of nanocrystals. The optimum amount of nanocrystalline phase differs for each group. In the case of magnetically hard nanocrystalline materials, full [20,25] or almost full [22,23] crystallization

* Tel.: +48-22 660 8399; fax: +48-22 660 8514.
*E-mail address:* tkulik@inmat.pw.edu.pl (T. Kulik).

0022-3093/01/$ - see front matter 
PII: S0022-3093(01)00627-5

Table 1
General characteristics of the three main groups of nanocrystalline materials produced by devitrification of metallic glasses ($V_{cr}$ – volume fraction of crystalline phase, $D$ – diameter of nanocrystals, $\lambda_s$ – saturation magnetostriction constant, $\langle K \rangle$ – averaged magnetocrystalline anisotropy, $\sigma_f$ – fracture strength)

| Nanocrystalline materials | Magnetically soft (Fe-based) | Constructional (Al-based) | Magnetically hard (Fe-based) |
|---|---|---|---|
| Alloys | Finemet® ($Fe_{73.5}Cu_1Nb_3Si_{13.5}B_9$) | Al–RE–TM (RE = Y, Ce, Nd, Sm; TM = Ni, Co, Fe, Cu) | Fe–RE–B |
| | Nanoperm® ($Fe_{84}Zr_{3.5}Nb_{3.5}B_8Cu_1$) | | e.g. $Fe_{82.3}Nd_{11.8}B_{5.9}$ $Fe_{88}Nb_2Pr_5B_5$ |
| | Hitperm ($Fe_{44}Co_{44}Zr_7B_4Cu_1$) | GIGAS® | |
| Structure | Nanocrystals (bcc-Fe) + Amorphous matrix | Amorphous matrix + Nanocrystals (fcc-Al) | Nanocrystals $Fe_{14}Nd_2B$ (+ $Fe_3B$, bcc-Fe, Am) |
| Sructural parameters | | | |
| $V_{cr}$ | 70–75% $\Rightarrow \lambda_s \approx 0$ | $\leqslant$40% $\Rightarrow$ ductility | $\leqslant$100% |
| $D$ | $\leqslant$15 nm $\Rightarrow \langle K \rangle \approx 0$ | $V_{cr} \uparrow$, $D \downarrow \Rightarrow \sigma_f \uparrow$ | <25 nm |
| Properties | High permeability, low magnetic losses | High specific strength at high temperatures | High coercivity, high remanence |

is required. For constructional and magnetically soft nanocrystalline materials the optimum mechanical and magnetic properties, respectively, are obtained after partial crystallization of their amorphous precursors [4,12], which means that they are two-phase materials composed of nanocrystals and an amorphous matrix. To preserve ductility in Al-based nanocrystalline alloys, $V_{cr}$ should not exceed 20% in ternary (Al–Y–Ni) [4] and 40% in quaternary (Al–Y–Ni–Cu) [9] alloys. Mechanical properties of these materials can be explained and predicted using mixture model based on the volume fractions of amorphous matrix and nanocrystals, proposed by Kim et al. [11]. GIGAS is a commercial name of Al-based nanocrystalline alloys with strength up to 1 GPa [26].

The most structure sensitive are properties of magnetically soft Fe-based nanocrystalline alloys. The volume fraction of nanocrystals should be the fraction which compensates their negative magnetostriction contribution by positive magnetostriction contribution of the amorphous matrix. A non-magnetostrictive Fe-based nanocrystalline material can be obtained for $V_{cr} = 70$–75%, depending on an alloy composition [27]. On the other hand, the diameter of nanocrystals, $D$, should be smaller than the magnetic exchange length in the crystalline phase to substantially reduce the contribution of magnetocrystalline anisotropy of this phase to the total magnetic anisotropy of a material [28]. According to random anisotropy model, developed by Herzer [28], the $D$ should not exceed about 15 nm in the case of α-Fe(Si) and α-Fe nanocrystals, present in Finemet [12] and Nanoperm [13] alloys, respectively.

Metallic glasses can be considered as materials which are kinetically metastable and thermodynamically unstable. Most of them are stable at temperatures close to room temperature and can be transformed to crystalline state at temperatures greater than room temperature. The onset temperature of the crystallization process, $T_x$, is called crystallization temperature and is usually determined during continuous heating with typical heating rates (10 to 20 K/min). The crystallization temperature as well as the mode of crystallization (primary, eutectic or polymorphous) are mainly dependent on an alloy composition [29]. The transformation from amorphous to fully crystalline state can proceed in one step (polymorphous and eutectic crystallization) or in several steps (primary crystallization). Crystallization of metallic glasses usually involves nucleation and growth processes [30]. To obtain nanoscale structure the crystallization process should proceed with the largest nucleation rate and the slowest crystal growth. Such conditions can be obtained for alloys with some compositions or by applying particular

methods of heat treatment. It was shown theoretically by Crespo et al. [31] and experimentally by Köster et al. [32] that metallic glasses with primary crystallization and with time-dependent long-range diffusion controlled growth rates are the most suitable candidates for nanocrystallization. Nevertheless, nanocrystalline structure was observed also for eutectically ($Pd_{60}Ti_{20}Si_{20}$ [33,34] and $Cu_{50}Ti_{40}Al_{10}$ [35]) and polymorphously ($Cu_{50}Ti_{40}Ni_{10}$ [35] and $Zr_{50}Co_{50}$ [36]) crystallizing glasses.

The subject of nanocrystallization of amorphous solids was summarized in 1996 by Lu [37]. More recently McHenry et al. [38] extensively reviewed the recent developments in the synthesis, structural characterization, properties and applications in the fields of amorphous and nanocrystalline magnetically soft materials.

The aim of this paper is to summarize briefly the current status of research in the field of nanocrystallization of metallic glasses, especially emphasizing the influence of glass composition and conditions of devitrification process on size, morphology and composition of crystallization products.

## 2. The role of glass composition in nanocrystallization process

Magnetically soft alloy with composition $Fe_{73.5}Cu_1Nb_3Si_{13.5}B_9$ and commercial name Finemet® [12] was the first nanocrystalline material obtained by crystallization of a metallic glass, with magnetic properties better than those found for the amorphous counterpart and therefore interesting from an applications point of view. Similar alloy with composition $Fe_{73.5}Cu_1Nb_3Si_{15.5}B_7$ is known as Vitroperm®. Nanoperm® is the next commercially available magnetically soft nanocrystalline alloy obtained using the same method. It was developed by Suzuki et al. [13], initially as Fe–Zr–B alloy. Finally, the best soft magnetic properties were found for the composition $Fe_{84}Zr_{3.5}Nb_{3.5}B_8Cu_1$ [16]. More recently (Fe,Co)–M–B–Cu (M = Zr, Nb or Hf) nanocrystalline alloys, called Hitperm, have been shown to have saturation magnetizations >1.6 T and Curie temperatures >1240 K [17,38,39]. Hitperm alloys are candidates for high-temperature soft-magnetic applications [17,39]. All these alloys can be transformed from amorphous to partially nanocrystalline state applying conventional annealing at temperatures close to crystallization temperatures. These alloys have a primary crystallization and are multicomponent. Each element has a particular effect. Silicon and boron are so called glass-forming elements, which facilitate forming the amorphous state of the alloys and increase thermal stability of amorphous phase. Iron and cobalt are the elements with magnetic moments and are the basic constituents of magnetic alloys. It is desirable to keep their content as large as possible to maximize magnetization of an alloy. Cobalt replacing iron increases magnetizations and Curie temperatures of both amorphous matrix and nanocrystals in Nanoperm-like (Fe–Zr–B–Cu) alloys [17,40,41]. In Finemet-like (Fe–Cu–Nb–Si–B) alloys only Curie temperature of nanocrystals increases whereas magnetizations of both phases decrease with the increase of cobalt content [41]. Copper, niobium and zirconium, despite their smaller concentrations in these alloys, affect the crystallization process and are responsible for nanocrystalline structure. Structures of Finemet® and Finemet-like alloys with missing copper and/or niobium, after conventional annealing for 1 h [42], are shown in Fig. 1. Nanocrystalline structure, with average grain diameter ~11 nm, is detected only in the alloys containing pairs of alloying elements (copper and niobium or copper and tantalum). The remaining alloys have larger crystallites. In the ternary Fe–Si–B alloy the crystals form dendrites with arm spans up to 300 nm. These results illustrate that under conventional conditions of annealing only metallic glasses with some compositions can be transformed into nanocrystalline material.

Copper, due to its very limited solubility in iron, forms small clusters, which can serve as sites for heterogeneous nucleation of Fe-based crystallites and increase their number by orders of magnitude. Hono et al. [43,44] have shown, using atom probe field ion microscopy (APFIM), that copper enriched clusters are formed prior to the onset of the crystallization process of Finemet. Ayers et al. [45]

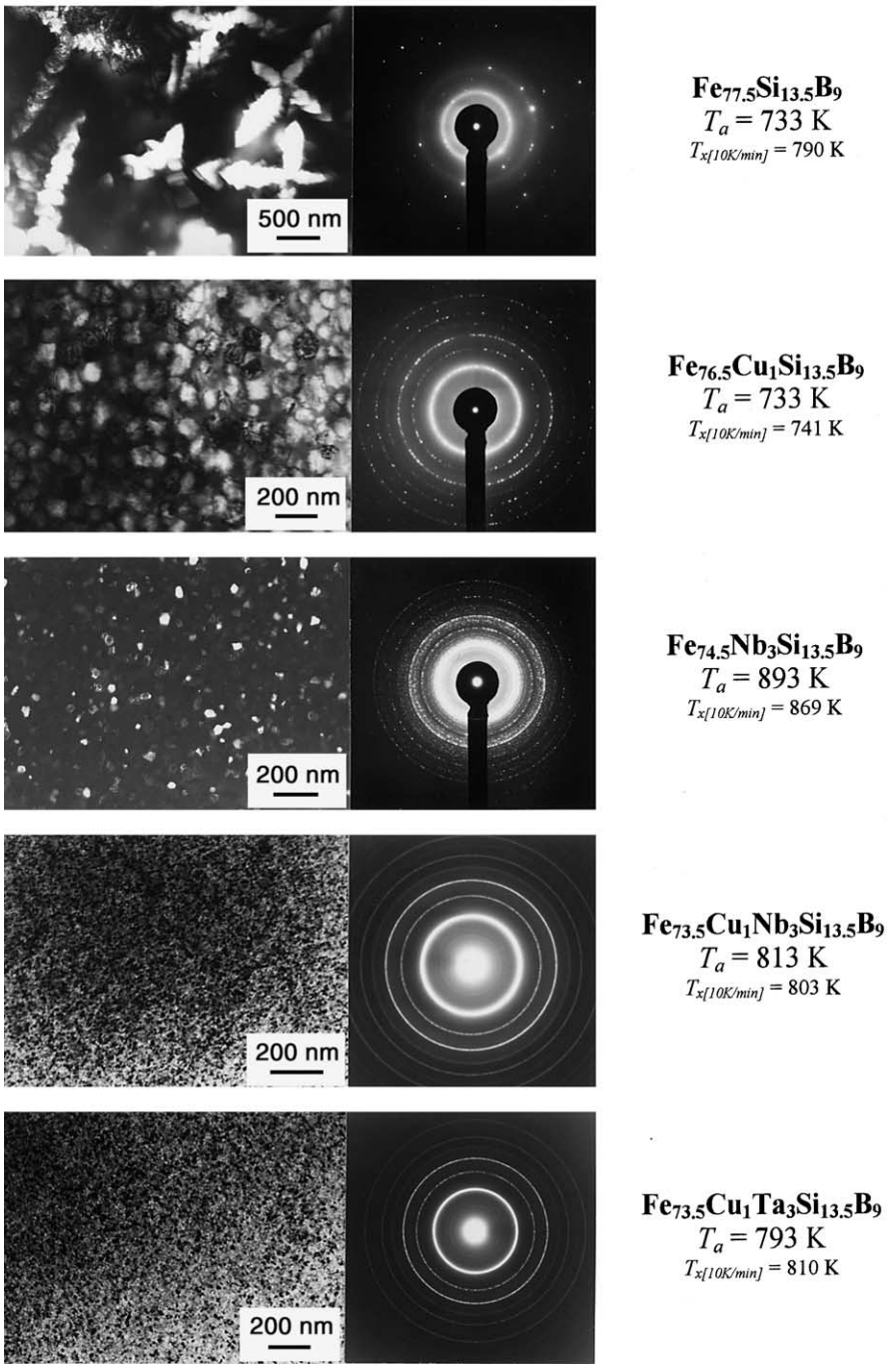


Fig. 1. Transmission electron micrographs and electron diffraction patterns of initially amorphous alloys after the first stage of crystallization obtained by conventional annealing at $T_a$ for 1 h [42]. ($T_x$ – crystallization onset temperature determined during continuous heating.)

reporting results of extended X-ray absorption fine structure (EXAFS) measurements also have shown that copper rich clusters with a near fcc structure form early in the precipitation process in $Fe_{73.5}Cu_1Nb_3Si_{13.5}B_9$ and $Fe_{76.5}Cu_1Si_{13.5}B_9$ glasses. Small angle neutron scattering (SANS) experiments allowed Ohnuma et al. [46] to estimate the average diameter and interparticle distance of copper enriched clusters in Finemet to be 1.8 and 6 nm, respectively. Copper clustering prior to the crystallization process was also observed (APFIM) by Zhang et al. [47] in Nanoperm alloys. Kataoka et al. [48] reported improvement of magnetic properties by addition of gold to Fe–Si–B–Nb alloy and concluded that grain refinement might have occurred. Duhaj et al. [49] have confirmed, using transmission electron microscopy (TEM), that gold has similar effect as copper on structure of Finemet-like alloys. Therefore, it can be stated that elements insoluble in iron, such as copper and gold, alter rate of heterogeneous nucleation and thus facilitate nanocrystallization of metallic glasses. However, recent report of Zhang and Zhu [50] shows that gold addition has no effect on nanocrystallization of Fe–Zr–B glasses. Different behaviour of gold in Fe–Si–B–Nb [48,49] and Fe–Zr–B [50] glasses can be attributed to much stronger attractive interactions between gold and zirconium then gold and niobium atoms. Predicted by Bakker [51] values of the interfacial enthalpy for gold solved in zirconium and niobium are $-294$ and $-134$ J/mol, respectively. Consequently, gold atoms do not cluster before the primary crystallization but co-segregation of gold and zirconium occurs during the growth of α-Fe crystallites without any influence on their nucleation and growth process [50].

On the other hand, elements such as niobium, tantalum and zirconium, which are rejected from a crystallization front to the amorphous matrix, decrease crystal growth because of relatively smaller diffusivity of big atoms of these elements in an amorphous phase [52]. According to Yavari and Drbohlav [53], the rejected atoms generate diffusion double-layers with larger concentration gradients. The layers also explain measured differences in Curie temperatures of the amorphous matrix in partially nanocrystalline alloy and fully amorphous alloy of the same composition as the matrix [53]. Results of EXAFS studies of nanocrystalline $Fe_{85}Zr_7B_6Cu_2$ alloy (Nanoperm®) indicate that the boundaries between α-Fe nanocrystallites and amorphous matrix are in the form of Fe-free interfaces with thickness of about 0.3 nm [54]. Recently reported results of SANS measurements of nanocrystalline $Fe_{73.5}Cu_1Nb_3Si_{15.5}B_7$ alloy (Vitroperm®) give experimental evidence for the accumulation of niobium atoms at the surface of α-Fe(Si) nanocrystallites [55]. These observations support the inhibitor concept of nanocrystallization of metallic glasses. Concentration of the elements controlling the growth rate of primary crystallites (e.g. Zr, Nb, Ta) in Nanoperm-type alloys is much larger (∼7 at.%) than in Finemet-type alloys (∼3 at.%). Probably, this difference is the reason that nanocrystalline structure can be obtained, using simple conventional annealing, in Cu-free Nanoperm-type alloys and cannot in Cu-free Finemet-type alloys. However, even in Nanoperm-type alloys the size of nanocrystallites can be reduced by copper addition and its influence increases with boron concentration, as was shown by Kopcewicz et al. [56]. Average diameter of α-Fe(Si) nanocrystallites in Finemet-type alloys does not exceed 15 nm after annealing (for 1 h) at temperatures up to ∼900 K and then increases [57,58] independently of boron and silicon concentrations in an alloy [57]. Evidently, the niobium addition in these alloys is responsible for the observed thermal stability of size of the nanocrystallites.

In Al-based alloys slowly diffusing elements with larger atomic radii in the amorphous matrix, that are insoluble in primary nanocrystals (α-Al), are rare earth elements [59–64] such as yttrium [8–11,62–64], cerium [59,62], neodymium [7,59,62], samarium [61] or ytterbium [65]. Nevertheless, their effectiveness in blocking growth of primary nanocrystals differs, e.g. Calin and Köster [63] have reported that partially nanocrystallized Nd-containing alloy ($Al_{90}Ni_6Nd_4$) is more stable against crystal coarsening than Y-containing alloy ($Al_{85}Ni_5Y_{10}$). The largest heterogeneous nucleation rates and number densities of nuclei observed during crystallization of Al–Ni–(Y, Ce, Nd) glasses [61] can be attributed to preferred

associations formed during melt spinning between component atoms (clusters) which serve as nucleants [59,62,64].

Hono and Ping recently reported results of APFIM studies of magnetically hard nanocrystalline $Fe_{73}Nd_{4.5}B_{18.5}Co_3Ga_1$ alloy and showed that cobalt and gallium atoms are rejected from $Fe_3B$ primary crystallites and control their growth by reducing the mobility at the crystal/amorphous interface [66].

Multicomponent alloys rich in zirconium have better glass-forming ability and can be produced in the amorphous state in a bulk form directly from the liquid, e.g. in Zr–Al–Cu–Ni [67], Zr–Ni–Cu–Ti [68] and Zr–Ni–Cu–Ti–Be [69] metallic systems. Greater strength bulk nanocrystalline materials can be produced by partial devitrification of bulk Zr-based glasses [70–72]. As was reported by Köster et al. [73] and Murty et al. [74], oxygen influences the crystallization process of Zr-based glasses. Presence of oxygen in $(Zr_{50}Co_{50})_{96}O_4$ glass incereases the formation of nanocrystalline structure by reduction of crystal growth rate and increase of nucleation rate by several orders of magnitude [73]. Results of APFIM studies of bulk amorphous $Zr_{65}Cr_{15}Al_{10}Pd_{10}$ alloy conducted by Chen et al. [75] showed that oxygen is uniformly distributed in the amorphous phase and its redistribution occurs during annealing. Impurity oxygen promotes crystallization and changes the crystallization mode by forming metastable phases containing oxygen. Increase of oxygen content above 0.4 at.% in $Zr_{65-x}Cu_{27.5}Al_{7.5}O_x$ glass results in formation of primary nano-quasicrystals instead of big polymorphic crystals of $Zr_2(Cu,Al)$ [74]. Chen et al. [76] recently showed that an icosahedral quasicrystalline phase with size $\sim$20 nm can be obtained during primary crystallization of bulk $Zr_{65}Al_{7.5}Ni_{10}Cu_{7.5}Ag_{10}$ glass. Löffler et al. [77] proposed model for nanocrystallization of undercooled bulk $Zr_{41.5}Ti_{13.8}Ni_{10}Cu_{12.5}Be_{22.5}$ glass. According to the model the glass first decomposes on the nanometer scale into two amorphous phases, increasing the nucleation probability, and later nanocrystallization occurs in one of the amorphous phases. A thermodynamic model for nanocrystallization in bulk metallic glasses was recently published by Desre [78].

## 3. The effects of annealing conditions on crystallization products

Fe-based Finemet®, Nanoperm® and their modifications, e.g. Vitroperm® and Hitperm as well as Al-based Gigas®, are nanocrystallizing metallic glasses and do not require any special heat treatment to be converted into nanocrystalline material [12,16,17,79]. They used to be transformed from amorphous to partially nanocrystalline state during simple isothermal annealing at temperature close to crystallization temperature in a time of, usually, 1 h. This kind of treatment can be called conventional nanocrystallization and is widely used by many researchers [80–90]. To determine susceptibility to nanocrystallization, especially of new alloys, it is useful to correlate microstructure and physical properties (magnetic or mechanical) with thermal properties of the glass. For this reason, heat treatment in a calorimeter applying continuous heating with a constant heating rate to a determined temperature, $T_{max}$, followed by cooling at a constant cooling rate is convenient. In this case $T_{max}$ is usually higher than the temperature of the end of the first crystallization step and less than the onset temperature of the second step of crystallization of the glass [79].

Both techniques of conventional nanocrystallization are effective only for those glasses which nanocrystallize more easily. It was found [91–94] that application of particular heat treatments makes possible nanocrystallization of any primarily crystallizing metallic glasses. Two different temperature regimes have been found to be useful for nanocrystallization of these metallic glasses: high-temperature [91,92] and low-temperature [93]. As already reported, by applying high temperature and very short time of annealing it is possible to create nanocrystalline structure even in ternary (Fe–Si–B [91] and Co–Si–B [92]) and binary (Fe–B [94,95]) glasses. Köster et al. [36] obtained nanocrystalline structure using high-temperature annealing also in polymorphously crystallizing $Zr_{50}Co_{50}$ glass. High-temperature nanocrystallization can be realized by flash annealing of amorphous ribbons using Joule heating [92,94]. Figs. 2 and 3 show the structures of par-

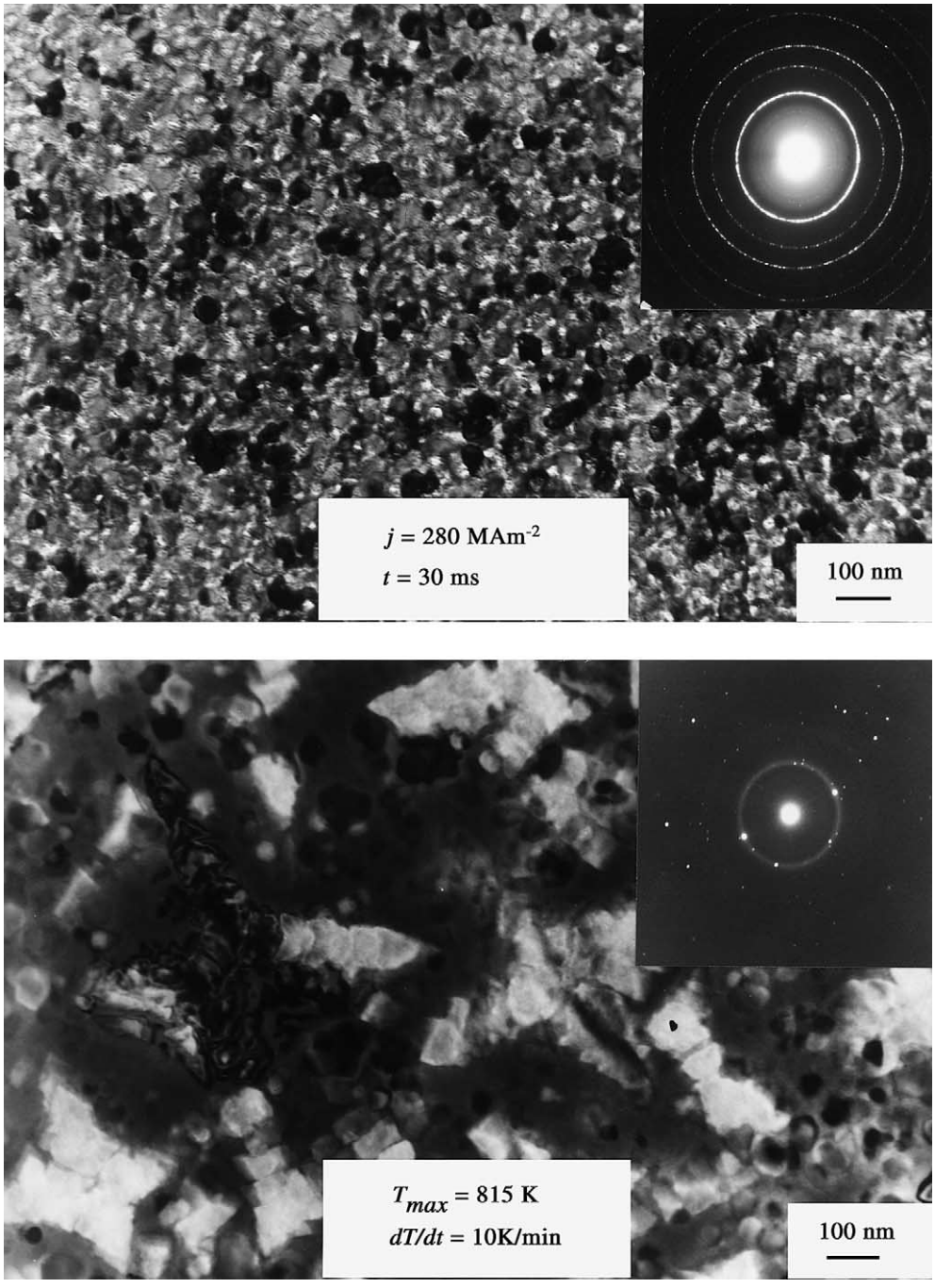


Fig. 2. Transmission electron micrographs and electron diffraction patterns of initially amorphous $Fe_{77.5}Si_{13.5}B_9$ alloy after the first stage of crystallization obtained by: conventional annealing during continuous heating from room temperature up to 815 K [79] and high-temperature flash annealing with current density $j = 280$ MA/m$^2$ and pulse time $t = 30$ ms [91].

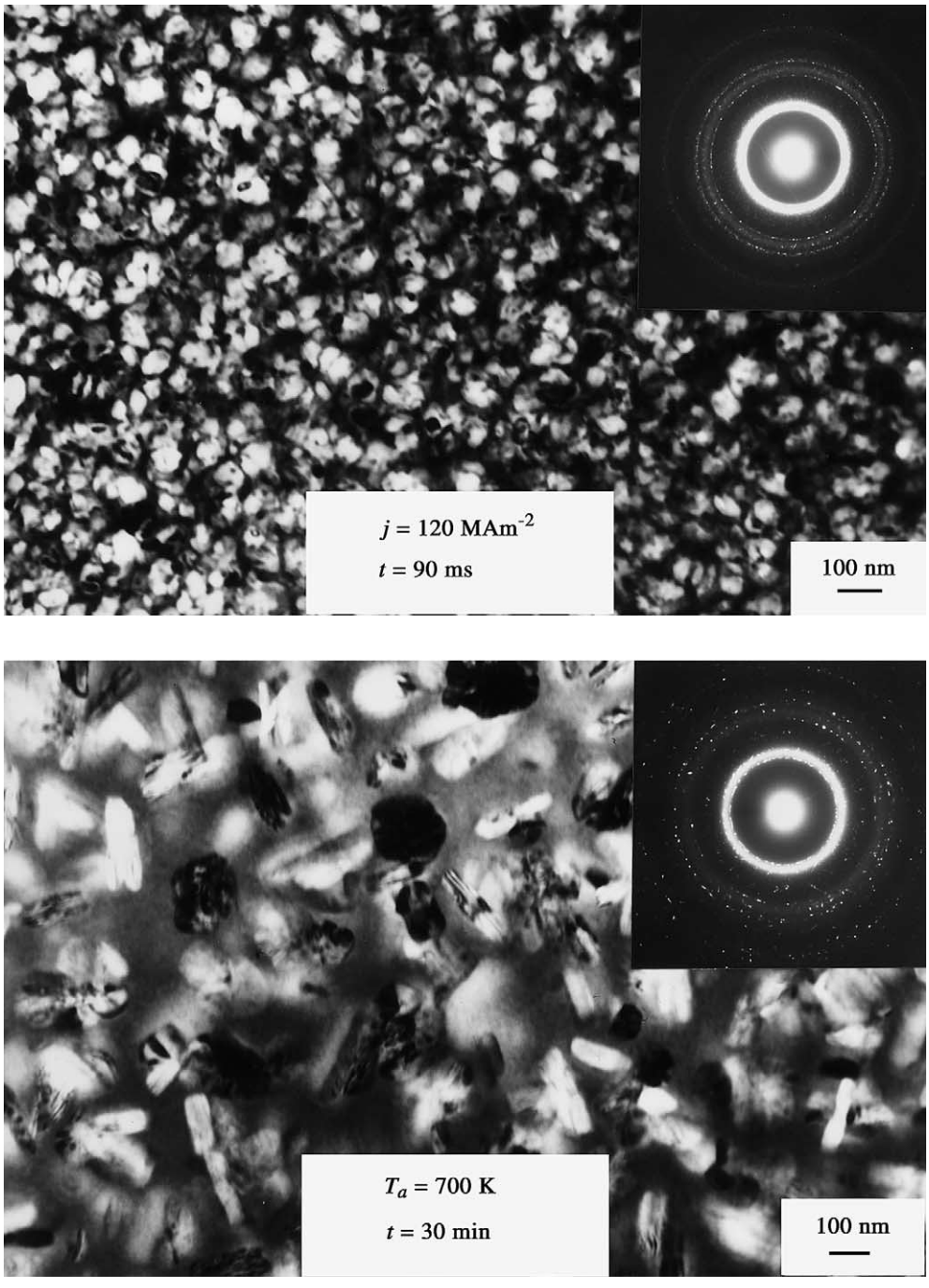


Fig. 3. Transmission electron micrographs and electron diffraction patterns of initially amorphous $Co_{78}Si_{11}B_{11}$ alloy after the first stage of crystallization obtained by: conventional isothermal annealing at 815 K for 30 min or high-temperature flash annealing with current density $j = 120$ MA/m$^2$ and pulse time $t = 90$ ms [92].

tially crystallized $Fe_{76.5}Si_{13.5}B_9$ and $Co_{78}Si_{11}B_{11}$ glasses, respectively, after conventional and flash annealing. It is evident from these figures that application of high-temperature annealing resulted in nanocrystalline structure for both alloys, whereas large crystals were observed after conventional annealing.

On the other hand, it was found [93,96–98] that application of relatively low temperature and longer annealing times also makes possible creation of nanocrystalline structure in ternary or even binary alloys. The influence of annealing temperature on size and morphology of α-Fe crystals in $Fe_{83}B_{17}$ glass after partial crystallization is presented in Fig. 4. The decrease of annealing temperature by 100 K resulted in much smaller crystals and a change in morphology of the crystals. Instead of dendrites with arms span ~100 nm, spherical crystals with average diameter ~35 nm are observed after annealing at the lower temperature.

Studies of metallic glasses after crystallization in a temperature range from 550 to 900 K revealed that size, morphology and composition of crystallization products depend on the annealing temperature [96]. Fig. 5 shows a wide spectrum of structures obtained in the same glass after annealing at different temperatures. The diffraction patterns confirm that in all the cases shown in Fig. 5, $Fe_{76.5}Cu_1Si_{13.5}B_9$ alloy is composed of bcc iron-based crystals and an amorphous matrix. Nevertheless, morphology and size of the crystals depend on the annealing temperature as shown in Fig. 5. The structure obtained after annealing at $T_a = 743$ K is typical for conventional crystallization of this alloy. Crystallization at higher $T_a$ results in smaller crystals. The top micrograph in Fig. 5 shows nanocrystalline structure obtained by high-temperature flash annealing. On the other hand, crystallization at lower $T_a$ results in larger crystals. When the annealing temperature is low enough the crystals become of such big size that they develop dendrites [93]. It was found that this change of morphology from spherulites to dendrites appears when the crystals exceed a critical size. The critical size depends on alloy composition and was observed to be ~130 and ~50 nm for $Fe_{76.5}Cu_1Si_{13.5}B_9$ and $Fe_{83}B_{17}$, respectively.

As seen in the bottom micrograph in Fig. 5, when the annealing temperature is below a critical temperature (~600 K for $Fe_{76.5}Cu_1Si_{13.5}B_9$ glass) again nanocrystalline structure can be obtained. The first results of prolonged (~300 h) annealing of metallic glasses at low temperatures (500–650 K) were published by Masumoto et al. [97], who obtained ultrafine structure for $Pd_{80}Si_{20}$, $Fe_{80}P_{13}C_7$, $Fe_{78}Si_{10}B_{12}$, $Co_{75}Si_{15}B_{10}$ and $Ni_{75}Si_8B_{17}$ alloys. Similar results were obtained by Thorpe et al. [98] for $Fe_{80}Ni_{40}P_{14}B_6$ alloy after annealing at 400 K for 1400 h and by Kulik et al. [93] for $Fe_{77.5}Si_{13.5}B_9$ after annealing at 573 K for 300 h. This effect can be explained assuming the existence in metallic glasses of small quenched-in clusters with short-range order close to a crystalline phase, which can serve as nuclei or sites for heterogeneous nucleation of crystals. It can be assumed that the clusters have a distribution in size in the range from $D_{min}$ up to $D_{max}$. As shown schematically in Fig. 6, if the annealing temperature $T_a$ is higher than $T_{a1}$ then all clusters are smaller than the critical cluster and, hence, all clusters are unstable and dissolve in an amorphous phase. When temperatures of conventional annealing exceed $T_{a1}$ quenched-in clusters do not participate in the crystallization process of metallic glasses. On the other hand, for $T_a < T_{a2}$ all clusters are bigger than the critical size and are stable and can serve as nuclei or nucleation sites. Therefore, the low-temperature nanocrystallization can be a result of existence of such clusters, which are nuclei and start to grow or are heterogeneous nucleation sites of new crystals.

Special method of low-temperature nanocrystallization of Fe–Si–B glasses, using high-current–density electropulsing, was proposed by Teng et al. [100] and Lai et al. [101]. Electropulsing of $Fe_{78}Si_9B_{13}$ glass for 30 min at average temperature ~673 K, which is substantially below the crystallization temperature ($T_{x\ (20\ K/min)} \approx 800$ K [102]), resulted in formation of primary α-Fe(Si) crystallites with average diameter of 23 nm [100]. However, the physical mechanism of electro-nanocrystallization is not yet understood [101]. On the other hand, by application of high pressure during crystallization of $Zr_{41}Ti_{14}Ni_9Cu_{12.5}Be_{22.5}C_1$ bulk glass Wang et al. [103] obtained very fine

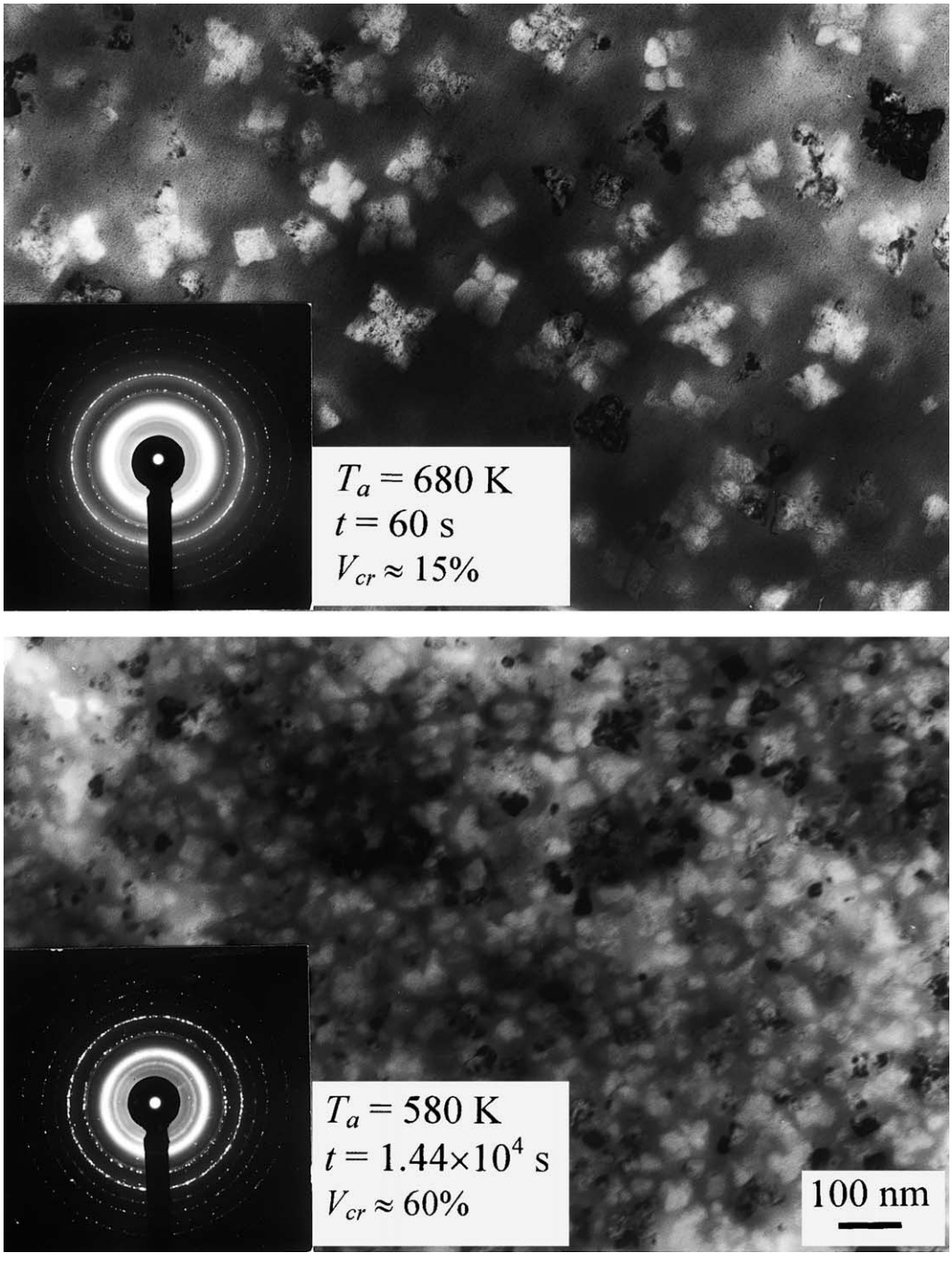


Fig. 4. Transmission electron micrographs and electron diffraction patterns of initially amorphous $Fe_{83}B_{17}$ alloy after conventional isothermal annealing at 680 K for 1 min or low-temperature annealing at 580 K for 4 h [99].

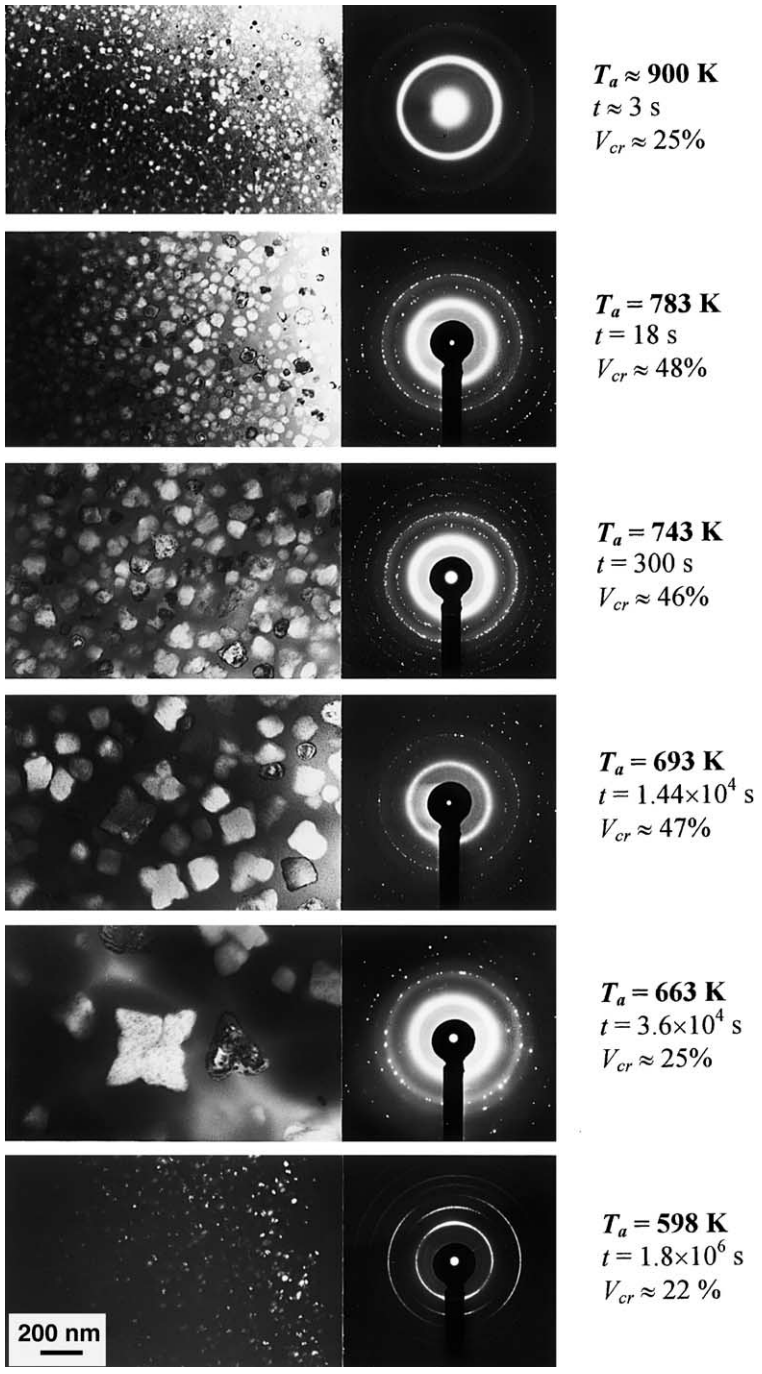


Fig. 5. Transmission electron micrographs and electron diffraction patterns of initially amorphous $Fe_{76.5}Cu_1Si_{13.5}B_9$ alloy after annealing at different temperatures $T_a$ for time $t$ [96].

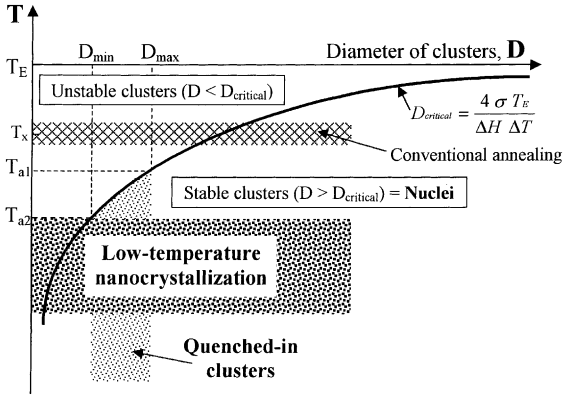


Fig. 6. Schematic diagram of temperature dependence of nucleus critical diameter $D_{\text{critical}}$ ($\sigma$-glass/crystal interfacial energy, $T_E$-equilibrium (melting) temperature, $T_a$-annealing temperature, $\Delta H$-crystallization enthalpy, $\Delta T = T_E - T_a$-undercooling).

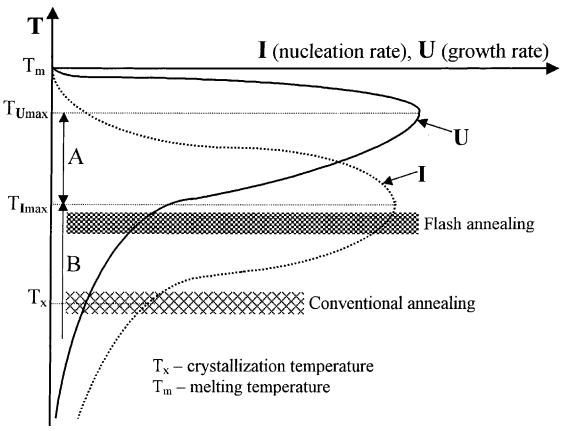


Fig. 7. Schematic diagram of temperature dependence of nucleation rate $I$ and growth rate $U$.

structure with primary crystallites less than 5 nm in diameter. The origin of the nanocrystallization phenomenon was attributed to the copious nucleation and slow crystal growth rate induced by high-pressure annealing. Moreover, it was observed [103] that the pressure reduced the crystallization temperature (by ~16 K/GPa) and determined the phase during the crystallization of the glass.

A possible explanation of the effect of high-temperature annealing on size of crystals appearing during crystallization of metallic glasses is presented in Fig. 7. As is known [104,105], the temperature of maximum growth rate, $T_{U\max}$, is less than the melting temperature, $T_m$, and the temperature of maximum nucleation rate, $T_{I\max}$, is much less than $T_m$. Solidification of liquid alloys usually takes place at $T > T_{I\max}$ (temperature range named **A** in Fig. 7) and crystallization of metallic glasses proceeds at $T_a < T_{I\max}$ (the range **B**). According to Fig. 7, an increase of annealing temperature, $T_a$, should be associated with much greater increase of nucleation rate, $I$, than growth rate, $U$. As a result of this difference, much finer structure will be present after high-temperature crystallization (flash-annealing) than after conventional crystallization.

Substantial reduction of crystal sizes, due to application of high-temperature annealing instead of conventional treatment, was observed also by Załuska et al. [94] in $Fe_{80}B_{20}$ and by Abrosimova et al. [95] in $Fe_{85}B_{15}$ and [106] $Fe_{82.5}B_{17.5}$ glasses. On the other hand, in the case of nanocrystallizing Finemet-type alloys [107,108] and Nanoperm-type alloys [109] both high-temperature annealing as well as conventional annealing led to similar nanocrystalline structure. Nevertheless, the mean size of nanocrystallites was slightly smaller after high-temperature crystallization [107–109].

High-temperature crystallization is most often realized using Joule heating and is called flash or current annealing. A model of Joule heating in amorphous metallic ribbons was developed by Allia et al. [110]. High-temperature nanocrystallization of metallic glasses using Joule heating was applied by many researchers to modify structure and improve properties of nanocrystalline materials. Allia et al. [111] have found that $Fe_{73.5}Cu_1Nb_3Si_{13.5}B_9$ after high-temperature nanocrystallization had a smaller brittleness (by ~30%) and larger initial permeability (by ~50%) than after conventional nanocrystallization. Larger initial permeability was also observed for $Fe_{83}Nb_7B_9Cu_1$ by Park et al. [112], who ascribed this effect to finer structure of the alloy after high-temperature nanocrystallization. Gorria et al. [113] reported much less brittleness of $Fe_{73.5}Cu_1Nb_3Si_{13.5}B_9$ and $Fe_{86}Cu_1Zr_7B_6$ alloys, supporting ten times greater tensile stress after flash annealing than after conventional annealing. Gupta et al. [108] attributed this effect to lower concentration of boron at the

amorphous/crystal interphase because a part of boron is retained inside the nanocrystals if they are formed during current annealing. Altoé et al. [114] reported that magnetically hard $Fe_{78}Nd_4B_{18}$ alloy after high-temperature nanocrystallization had larger remanence (by 12%) and coercivity (by 20%) than the same alloy crystallized conventionally. Kojima et al. [115] performed high-temperature crystallization of amorphous Fe–Co–Nb–(Nd, Pr)–B alloys using rapid heating (with rates up to 3 K/s) in an infrared furnace. Such treatment caused refinement of both primary α-Fe phase and also $Nd_2Fe_{14}B$ phase which precipitates subsequently around the former phase. Consequently the improvement of hard magnetic properties of these Fe-rich nanocomposite materials was achieved [115].

The size, morphology of crystallites and the mechanism of crystallization and crystallization products themselves can depend on the temperature of devitrification of a metallic glass. Recently, Illekova and Duhaj [116] reported for $Fe_{53.5}Ni_{20}Cu_1Nb_3Si_{13.5}B_9$ glass a change of crystallization mode from primary to eutectic, when the heating rate was increasing above 20 K/min, which was a consequence of the shift of crystallization process to higher temperatures. Załuska and Matyja [117] have found that applying high-temperature (flash) annealing a change of crystallization mode from polymorphous (γ phase) to eutectic (α + γ phases) can be obtained in $Fe_{45}Ni_{35}Si_{10}B_{10}$ and $Fe_{40}Ni_{40}Si_{10}B_{10}$ glasses. Abrosimova et al. [106] have observed a change of space-group of $Fe_3B$ tetragonal lattice from $\bar{I}4$ to $P4_2/n$ with the increase of annealing temperature using Joule heating.

The annealing temperature also influences the composition of crystallization products. This effect is indirectly dectected by changing lattice parameter, $a$, of the crystalline phase with change of annealing temperature, as shown in Fig. 8. Annealing of $Fe_{76.5}Cu_1Si_{13.5}B_9$ glass at temperatures higher than 650 K results in formation of α-Fe(Si) (bcc solid solution of silicon in iron) with lattice parameter considerably less than that (0.2866 nm) [118] for pure α-Fe. This effect is commonly known of smaller size of silicon atoms (than iron atoms) forming with iron a substitutional solid solution. From the experimentally determined relation between $a$ and silicon concentration in α-Fe(Si) [118] I estimate that crystals formed in $Fe_{76.5}Cu_1Si_{13.5}B_9$ glass at $T_a > 650$ K contain 14–17 at.% of silicon, depending on their volume fraction. Thus the concentration of silicon in primary crystals is close to its relative (in relation to iron) concentration in the alloy, for which $C_{Si}/(C_{Si} + C_{Fe}) = 0.15$. As seen in Fig. 8, a decrease of $T_a$ results in an increase of $a$ indicating that α-Fe(Si) crystallites become progressively depleted in silicon, which is correlated to decreasing solubility of silicon in iron. Similar effect was observed for Fe–Si–B glasses by Mattern et al. [119] and Ueda et al. [120] and for Finemet-type Fe–Cu–Nb–Si–B alloys by Battezzati and Baricco [121] and Borrego et al. [122].

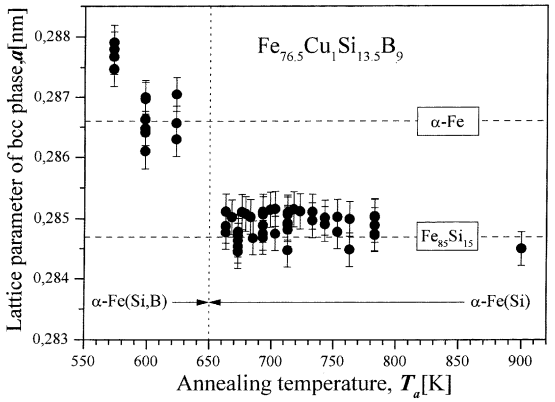


Fig. 8. Influence of devitrification temperature $T_a$ on lattice parameter $a$ of primary crystals in initially amorphous $Fe_{76.5}Cu_1Si_{13.5}B_9$ alloy [96].

As seen in Fig. 8, for $T_a \leqslant 650$ K the lattice parameter of the bcc phase exceeds that for pure α-Fe. This effect is explained by assuming that the crystalline phase is not only a substitutional solid solution of silicon in iron but also an interstitial solid solution of boron in iron. Formation of supersaturated solid solution of boron in α-Fe was observed by Duhaj and Hanic [123] during crystallization of $Fe_{86}B_{14}$ and $Fe_{84}B_{16}$ glasses. Therefore, the observed increase of $a$ with the decrease of $T_a$ can be explained by a decrease of silicon content or/and an increase of boron content in α-Fe(Si,B) phase. In the case of Finemet-type alloys the dependence of $a$ on $T_a$ can be additionally related to niobium atoms entrapped in α-Fe(Si,B) nanocrystals. Similar effect of entrapping atoms of

insoluble element in a basic constituent (solvent) of an alloy, related to crystallization of a metallic glass at relatively low temperatures, was observed also in $Al_{90}Y_{10}$ and $Al_{80}Y_5Ni_{15}$ alloys [124]. For example, in $Al_{90}Y_{10}$ glass heated continuously to the temperature of the maximum of the first calorimetric peak, the lattice parameter $a$ of fcc α-Al(Y) phase increased from 0.4065 to 0.4078 nm with the decrease of maximum annealing temperature from 540 to 440 K (when heating rate was decreased from 200 to 2 K/min). Both $a$s for α-Al(Y) are greater than that (0.4049 nm) [125] for pure α-Al. This effect is associated with the bigger size of yttrium atoms (0.181 nm in diameter) than aluminium atoms (0.142 nm). Larger $a$ indicates greater content of yttrium in α-Al(Y) after crystallization at lower temperature. I conclude that composition of primary crystals is dependent on temperature of devitrification process and the lower the annealing temperature the more the crystals composition differs from the equilibrium state.

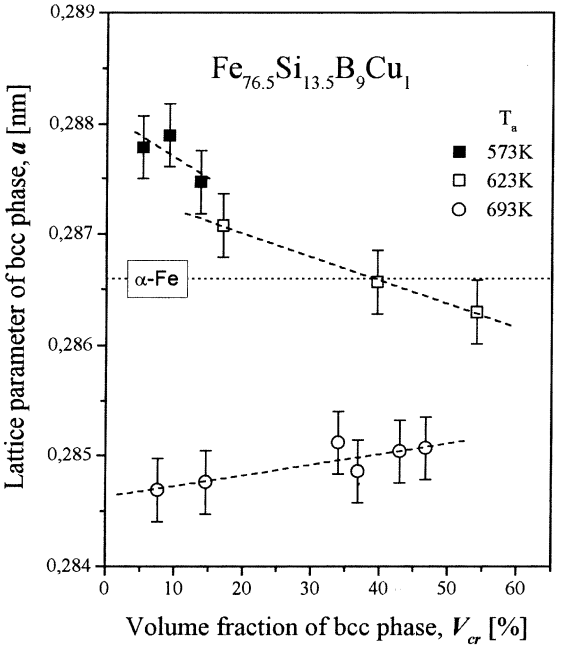


Fig. 9. Dependence of lattice parameter $a$ of primary crystals on their volume fraction $V_{cr}$ (annealing time) in initially amorphous $Fe_{76.5}Cu_1Si_{13.5}B_9$ alloy after isothermal annealing at different temperatures $T_a$ [99].

The composition of primary crystals changes also with annealing time. Fig. 9 shows the dependence of $a$ on volume fraction, $V_{cr}$, of bcc phase in $Fe_{76.5}Cu_1Si_{13.5}B_9$ alloy after isothermal annealing at different temperatures. These results can be explained assuming that concentrations of the solute elements (silicon and boron) decrease with increase of $V_{cr}$ or in other words with increase of annealing time. At high temperatures (693 K) mainly silicon is dissolved in iron and a decrease of its concentration in α-Fe(Si) with annealing time should result in the observed increase of $a$. On the other hand, at low temperatures (573 and 623 K) boron in α-Fe(Si,B) can be expected by me and the decrease of its content with annealing time should result in the observed decrease of $a$ of this phase. Remarkable decrease of $a$ of primary phase with the annealing time was observed also for Finemet-type Fe–Cu–Nb–Si–B alloys [36,121,122,126]. On the other hand, Curie temperature $T_c$ of the nanocrystalline phase in Finemet® increases with the annealing time [127]. These changes of $a$ and $T_c$ indicate a significant change in the composition with increasing size of primary nanocrystals. It is very probable that small Fe-based nanocrystallites are supersaturated by all alloying elements and tend to the equilibrium state during crystallization process. Barquín et al. [126] observed that composition stabilization of Fe(Si) nanocrystals during crystallization process of $Fe_{73.5}Cu_1Nb_3Si_{13.5}B_9$ glass was achieved after 1 h annealing at 773 K. Therefore, it can be concluded that the increase of annealing time of a metallic glass results not only in a larger volume fraction of crystalline phase and size of crystallites but also in a composition of the phase closer to the equilibrium state.

## 4. Conclusions

The possibility of nanocrystalline phase creation by crystallization of metallic glasses depends mainly on the alloy composition and temperature of the process. Conventional crystallization enables the creation of nanocrystalline structure only in glasses with a specific composition. Two non-conventional methods of nanocrystallization of metallic glasses can be applied: (1) high-temperature

nanocrystallization using flash annealing followed by fast cooling, and (2) low-temperature nanocrystallization, by prolonged annealing at temperatures below the critical temperature. With these methods it is possible to form nanocrystalline structure in any metallic glass having a primary crystallization process.

Temperature of devitrification process influences sizes and compositions of crystallization products for any volume fraction of crystalline phase. The change of crystallites sizes can lead to a change in their morphology, e.g. from spherulites to dendrites, when the crystallites exceed a critical size ($\sim$50 and $\sim$130 nm for $Fe_{83}B_{17}$ and $Fe_{76.5}Cu_1$ $Si_{13.5}B_9$ alloys, respectively). The change of a crystallite composition usually affects the lattice parameter but also can result in a change of crystallographic structure of the same phase or in formation of another phase. Annealing temperature sometimes determines the type of crystallization process (primary, eutectic or polymorphous).

Composition of primary crystallites is dependent on temperature as well as on time of devitrification process. The lower the annealing temperature and the shorter the annealing time (smaller crystallites) the more the crystallites composition differs from the equilibrium state.

## References


[1] C. Suryanarayana, Int. Mater. Rev. 40 (1995) 41.
[2] B. Cantor, Mater. Sci. Forum 307 (1999) 143.
[3] A.L. Greer, Mater. Sci. Forum 269–272 (1998) 3.
[4] A. Inoue, K. Ohtera, A.-P. Tsai, T. Masumoto, Jpn. J. Appl. Phys. 27 (1988) L280.
[5] Y.H. Kim, A. Inoue, T. Masumoto, Trans. JIM 31 (1990) 747.
[6] H. Chen, Y. He, G.J. Shiflet, S.J. Poon, Scr. Metall. 25 (1991) 1421.
[7] J.H. Paik, F.W.J. Botta, A.R. Yavari, Mater. Sci. Forum 225–227 (1996) 305.
[8] Z.C. Zhong, X.Y. Jiang, A.L. Greer, Mater. Sci. Eng. A 226–228 (1997) 531.
[9] J. Latuch, A. Kokoszkiewicz, H. Matyja, Mater. Sci. Eng. A 226–228 (1997) 809.
[10] Z.C. Zhong, X.Y. Jiang, A.L. Greer, Philos. Mag. 76 (1997) 505.
[11] H.S. Kim, P.J. Warren, B. Cantor, H.R. Lee, Nanostr. Mater. 11 (1999) 241.
[12] Y. Yoshizawa, S. Oguma, K. Yamauchi, J. Appl. Phys. 64 (1988) 6044.
[13] K. Suzuki, N. Kataoka, A. Inoue, T. Masumoto, Mater. Trans. JIM 31 (1990) 743.
[14] K. Suzuki, A. Makino, A. Inoue, T. Masumoto, J. Appl. Phys. 74 (1993) 3316.
[15] H.K. Lachowicz, A. Ślawska-Waniewska, J. Magn. Magn. Mater. 133 (1994) 238.
[16] A. Makino, T. Bitoh, A. Inoue, T. Masumoto, J. Appl. Phys. 81 (1997) 2736.
[17] M.A. Willard, D.E. Laughlin, M.E. McHenry, D. Thoma, K. Sickafus, J.O. Cross, V.G. Harris, J. Appl. Phys. 84 (1998) 6773.
[18] R. Coehoorm, D.B. De Mooiji, J.P.W.B. Duchateau, K.H.J. Buschow, J. Phys. 49 (1988) 699.
[19] E.F. Kneller, R. Hawing, IEEE Trans. Magn. 27 (1991) 3588.
[20] A. Manaf, R.A. Buckly, H.A. Davies, J. Magn. Magn. Mater. 128 (1993) 302.
[21] L. Withanawasam, A.S. Murphy, G.C. Hadjipanayis, R.F. Krause, J. Appl. Phys. 78 (1994) 7065.
[22] A. Inoue, A. Takeuchi, A. Makino, T. Masumoto, Mater. Trans. JIM 36 (1995) 676.
[23] A. Inoue, A. Takeuchi, A. Makino, T. Masumoto, Mater. Trans. JIM 36 (1995) 962.
[24] T. Hopfinger, A.R. Yavari, D. Negri, J. Alonso, A. Hernando, J. Magn. Magn. Mater. 164 (1996) L7.
[25] A. Takeuchi, A. Inoue, A. Makino, Mater. Sci. Eng. A 226–228 (1997) 636.
[26] A. Inoue, H. Kimura, Mater. Sci. Eng. A 286 (2000) 1.
[27] T. Kulik, G. Vlasák, R. Żuberek, Mater. Sci. Eng. A 226–228 (1997) 701.
[28] G. Herzer, IEEE Trans. Magn. MAG-25 (1989) 3327.
[29] U. Herold, U. Köster, in: B. Cantor (Ed.), Proceedings of the Third International Conference Rapidly Quenched Metals, vol. I, Metals Society, London, 1978, p. 281.
[30] U. Köster, U. Herold, in: H.J. Güntherodt, H. Beck (Eds.), Glassy Metals I, Topics in Applied Physics, vol. 46, Springer, Berlin, 1981, p. 225.
[31] D. Crespo, T. Pradell, N. Clavaguera, M.T. Clavaguera-Mora, Mater. Sci. Eng. A 238 (1997) 160.
[32] U. Köster, U. Schünemann, M. Blank-Bewersdorff, S. Brauer, M. Sutton, G.B. Stephenson, Mater. Sci. Eng. A 133 (1991) 611.
[33] L. Battezzati, C. Antonione, G. Riontino, F. Marino, H.R. Sinning, Acta Metall. Mater. 39 (1991) 2107.
[34] M. Baricco, L. Battezzati, Mater. Sci. Forum 179–181 (1995) 597.
[35] W.N. Myung, L. Battezzati, M. Baricco, K. Oaki, A. Inoue, T. Masumoto, Mater. Sci. Eng. A 179&180 (1994) 371.
[36] U. Köster, J. Meinhardt, Mater. Sci. Eng. A 178 (1994) 271.
[37] K. Lu, Mater. Sci. Eng. R 16 (1996) 161.
[38] M.E. McHenry, M.A. Willard, D.E. Laughlin, Prog. Mater. Sci. 44 (1999) 291.
[39] H. Iwanabe, B. Lu, M.E. McHenry, D.E. Laughlin, J. Appl. Phys. 85 (1999) 4424.

[40] S. He, K. He, B. Shen, H. Zhang, S. Zhang, H. Guo, J. Appl. Phys. 86 (1999) 6301.
[41] M. Müller, H. Grahl, N. Mattern, U. Kühn, B. Schnell, J. Magn. Magn. Mater. 160 (1996) 284.
[42] T. Kulik, Magnetically Soft Nanocrystalline Materials Obtained by the Crystallization of Metallic Glasses, Publishing House of Warsaw University of Technology, Warsaw, 1998, p. 38 (in Polish).
[43] K. Hono, K. Hiraga, Q. Wang, A. Inoue, T. Sakurai, Acta Metall. Mater. 40 (1992) 2137.
[44] K. Hono, J.-L. Li, Y. Ueki, A. Inoue, T. Sakurai, Appl. Surf. Sci. 67 (1993) 398.
[45] J.D. Ayers, V.G. Harris, J.A. Sprague, W.T. Elam, H.N. Jones, Acta Mater. 46 (1998) 1861.
[46] M. Ohnuma, K. Hono, H. Onodera, J.S. Pedersen, S. Linderoth, Nanostr. Mater. 12 (1999) 693.
[47] Y. Zhang, K. Hono, A. Inoue, T. Sakurai, Scr. Mater. 34 (1996) 1705.
[48] N. Kataoka, T. Matsunaga, A. Inoue, T. Masumoto, Mater. Trans. JIM 30 (1989) 947.
[49] P. Duhaj, P. Švec, D. Janičkovič, I. Mat'ko, Mater. Sci. Eng. A 133 (1991) 398.
[50] Y. Zhang, F. Zhu, J. Mater. Res. 15 (2000) 1271.
[51] H. Bakker, in: M. Magini, H. Wöhlbier (Eds.), Materials Science Foundations vol. 1: Enthalpies in Alloys, TransTech, Aedermannsdorf, 1998, p. 69.
[52] R.W. Cahn, in: R.W. Cahn, P. Haasen, E.J. Kramer (Eds.), Materials Science and Technology, vol. 9: Glassses and Amorphous Materials, VCH, Weinheim, 1991, p. 493.
[53] A.R. Yavari, O. Drbohlav, Mater. Trans. JIM 36 (1995) 896.
[54] Y. Swilem, E. Sobczak, R. Nietubyć, P. Dłużewski, A. Ślawska-Waniewska, J. Alloys Comp. 286 (1999) 103.
[55] H. Hermann, A. Heinemann, N. Mattern, A. Wiedenmann, Europhys. Lett. 51 (2000) 127.
[56] M. Kopcewicz, A. Grabias, D.L. Williamson, J. Appl. Phys. 82 (1997) 1747.
[57] T. Kulik, A. Hernando, Mater. Sci. Forum 179–181 (1995) 587.
[58] S.D. Kaloshkin, Mater. Sci. Forum 307 (1999) 119.
[59] A.R. Yavari, O. Drbohlav, Mater. Sci. Forum 225–227 (1996) 295.
[60] J.C. Foley, D.R. Allen, J.H. Perepezko, Mater. Sci. Eng. A 226–228 (1997) 569.
[61] T. Gloriant, A.L. Greer, Nanostr. Mater. 10 (1998) 389.
[62] M. Calin, A. Rüdiger, U. Köster, Mater. Sci. Forum 343–346 (2000) 359.
[63] M. Calin, U. Köster, Mater. Sci. Forum 269–272 (1998) 749.
[64] S. Saini, A. Zaluska, Z. Altounian, J. Non-Cryst. Solids 250–252 (1999) 714.
[65] G.E. Abrosimova, A.S. Aronin, Yu.V. Kir'janov, T.F. Gloriant, A.L. Greer, Nanostr. Mater. 12 (1999) 617.
[66] K. Hono, D.H. Ping, Mater. Sci. Forum 307 (1999) 69.
[67] A. Inoue, T. Zhang, T. Masumoto, Mater. Trans. JIM 31 (1990) 177.
[68] V.V. Molokanov, V.N. Chebotnikov, Key Eng. Mater. 41&42 (1990) 319.
[69] A. Pecker, W.L. Johnson, Appl. Phys. Lett. 63 (1993) 2342.
[70] A. Inoue, C. Fan, Nanostr. Mater. 12 (1999) 741.
[71] A. Inoue, C. Fan, A. Takeuchi, J. Non-Cryst. Solids 250–252 (1999) 724.
[72] A. Inoue, Intermetallics 8 (2000) 455.
[73] U. Köster, A. Rüdiger, J. Meinhardt, Mater. Sci. Forum 307 (1999) 9.
[74] B.S. Murty, D.H. Ping, K. Hono, A. Inoue, Acta Mater. 48 (2000) 3985.
[75] M.W. Chen, A. Inoue, T. Sakurai, D.H. Ping, K. Hono, Appl. Phys. Lett. 74 (1999) 812.
[76] M.W. Chen, A. Inoue, T. Zhang, A. Sakai, T. Sakurai, Intermetalics 8 (2000) 493.
[77] J. Löffler, W.L. Johnson, Appl. Phys. Lett. 76 (2000) 3394.
[78] P.J. Desre, Philos. Mag. 80 (2000) 401.
[79] T. Kulik, Mater. Sci. Eng. A 159 (1992) 95.
[80] G. Herzer, IEEE Trans. Magn. MAG-26 (1990) 1397.
[81] T.H. Noh, M.B. Lee, H.J. Kim, I.K. Kang, J. Appl. Phys. 67 (1990) 5568.
[82] M. Müller, N. Mattern, L. Illgen, Z. Metallkd. 82 (1991) 895.
[83] M. Vázquez, P. Marín, J. González, A. Hernando, E. Pulido, in: A. Conde, C.F. Conde, M. Millán (Eds.), Trends in Non-Crystalline Solids, World Scientific, Singapore, 1992, p. 157.
[84] C. Polak, R. Grössinger, H. Sassik, G. Herzer, J. Magn. Magn. Mater. 104–107 (1992) 100.
[85] I. Škorvánek, R. Gerling, J. Appl. Phys. 72 (1992) 3417.
[86] C. Wittwer, W. Riehemann, W. Heye, J. Magn. Magn. Mater. 133 (1994) 287.
[87] J. Bigot, N. Lecaude, J.C. Perron, C. Milan, C. Ramiarinjaona, J.F. Rialland, J. Magn. Magn. Mater. 133 (1994) 299.
[88] Z. Wang, K. He, S. He, Y. Zhang, Y. Fu, L. Zhang, J. Magn. Magn. Mater. 171 (1997) 300.
[89] V. Franco, C.F. Conde, A. Conde, J. Appl. Phys. 84 (1998) 5108.
[90] M. Miglierini, M. Kopcewicz, B. Idzikowski, Z.E. Horváth, A. Grabias, I. Škorvánek, P. Duźewski, Cs.S. Daróczi, J. Appl. Phys. 85 (1999) 1014.
[91] T. Kulik, T. Horubała, H. Matyja, Mater. Sci. Eng. A 157 (1992) 107.
[92] T. Kulik, D. Bucka, H. Matyja, J. Mater. Sci. Lett. 12 (1993) 76.
[93] T. Kulik, J. Ferenc, H. Matyja, Mater. Sci. Forum 235–238 (1997) 421.
[94] A. Załuska, L. Załuski, A. Witek, Mater. Sci. Eng. 89 (1989) 11.
[95] G.E. Abrosimova, A.S. Aronin, V.A. Stelmuh, Solid State Phys. 33 (1991) 3570 (in Russian).
[96] T. Kulik, Mater. Sci. Forum 269–272 (1998) 707.
[97] T. Masumoto, H. Kimura, A. Inoue, Y. Waseda, Mater. Sci. Eng. 23 (1976) 141.
[98] S.J. Thorpe, B. Ramaswami, K.T. Aust, Acta Metall. 36 (1988) 795.
[99] T. Kulik, unpublished data.

[100] G.Q. Teng, Y.S. Chao, Y. Geng, L. Dong, Z.H. Lai, Jpn. J. Appl. Phys. 35 (1996) 5320.
[101] Z.H. Lai, H. Conrad, G.Q. Teng, Y.S. Chao, Mater. Sci. Eng. A 287 (2000) 238.
[102] N. DeCristofaro, A. Freilich, G. Fish, J. Mater. Sci. 17 (1982) 2365.
[103] W.H. Wang, D.W. He, D.Q. Zhao, Y.S. Yao, M. He, Appl. Phys. Lett. 75 (1999) 2770.
[104] U. Köster, J. Meinhardt, H. Alves, Mater. Sci. Forum 179–181 (1995) 533.
[105] A.L. Greer, Metall. Mater. Trans. 27A (1996) 549.
[106] G.E. Abrosimova, A.S. Aronin, A.V. Bezrukov, S.P. Pankratov, A.V. Serebriakov, Metallofizika 4 (1982) 69 (in Russian).
[107] R. Houssa, V. Franco, A. Conde, J. Magn. Magn. Mater. 203 (1999) 199.
[108] A. Gupta, N. Bhagat, G. Principi, A. Maddalena, N. Malhotra, B.A. Dasannacharya, P.S. Goel, H. Amenitsch, S. Bernstorff, Intermetallics 8 (2000) 287.
[109] F.C.S. da Silva, E.F. Ferrari, M. Knobel, I.L. Torriani, D.R. dos Santos, Appl. Phys. Lett. 77 (2000) 1375.
[110] P. Allia, M. Baricco, M. Knobel, P. Tiberto, F. Vinai, Mater. Sci. Eng. A 179&180 (1994) 361.
[111] P. Allia, P. Tiberto, M. Baricco, F. Vinai, Appl. Phys. Lett. 63 (1993) 2759.
[112] J.Y. Park, K.Y. Kim, T.H. Noh, M.B. Lee, S.J. Suh, Mater. Sci. Eng. A 226–228 (1996) 685.
[113] P. Gorria, I. Orue, F. Plazaola, J.M. Barandiarán, J. Appl. Phys. 73 (1993) 6600.
[114] M.V.P. Altoé, M.S. Lancarotte, H.R. Rechenberg, F.P. Missell, J.M. González, IEEE Trans. Magn. 31 (1995) 3614.
[115] A. Kojima, A. Makino, A. Inoue, J. Appl. Phys. 87 (2000) 6576.
[116] E. Illekova, P. Duhaj, Acta Phys. Slovaca 50 (2000) 525.
[117] A. Załuska, H. Matyja, Mater. Sci. Eng. 97 (1988) 347.
[118] W.B. Pearson, Lattice Spacings and Structures of Metals, vol. II, Pergamon, London, 1967, p. 935.
[119] N. Mattern, A. Danzig, M. Müller, Mater. Sci. Eng. A 194 (1995) 77.
[120] Y. Ueda, S. Ikeda, Y. Minami, Mater. Sci. Eng. A 181&182 (1994) 992.
[121] L. Battezzati, M. Baricco, Philos. Mag. 68 (1993) 813.
[122] J.M. Borrego, C.F. Conde, M. Millán, A. Conde, M.J. Capitán, J.L. Joulaud, Nanostr. Mater. 10 (1998) 575.
[123] P. Duhaj, F. Hanic, Phys. Status Solid 76 (1983) 467.
[124] T. Kulik, J. Latuch, Mater. Sci. Forum 360–362 (2001) 149.
[125] ASTM Card No. 4-787.
[126] L.F. Barquín, J.C. Gómez Sal, P. Gorria, J.S. Garitaonandia, J.M. Barandiaran, J. Phys.: Condens. Matter. 10 (1998) 5027.
[127] M.S. Leu, T.S. Chin, I.C. Tung, C.M. Lee, Jpn. J. Appl. Phys. 38 (1999) 707.